Fifth International Symposium on Marine Propulsors
smp'17, Espoo, Finland, June 2017

Panel method for ducted propellers with sharp and round trailing edge duct with fully aligned wake on blade and duct

Seungnam Kim, Weikang Du, Spyros A. Kinnas[1]

[1]Ocean Engineering Group, Department of Civil, Architectural and Environmental Engineering, The University of Texas at Austin, Austin, Texas, USA

ABSTRACT

In this paper, an improved extension scheme, which is based on the viscous/inviscid interaction method, is proposed to extend the bare duct with round trailing edge to sharp trailing edge with consideration of the flow separation. It is assumed that the pressure in the extended part is constant, from which come the criteria that the force and moment differences should be zero from the extended inner and outer sides. A two-dimensional Newton-Raphson method is used, and the pressure distributions and skin friction on the duct the extension scheme are compared with the results obtained from RANS simulation.

A low order panel method is also applied to predict the performance of the ducted propeller with Full Wake Alignment (FWA) on duct wake. Now that the free vortex sheets shed from the trailing edge of a duct are the material surface, which has to be aligned based on the local flow velocity, duct wake is fully aligned based on FWA. This paper will present the basic algorithm built in FWA. Then, correlations between the predicted results from the panel method and RANS simulations will be investigated. Experimental data are also adopted for the further validation of the results from the panel method.

Keywords

Ducted propeller, panel method, boundary layer separation, blunt trailing edge extension, duct wake alignment.

1 INTRODUCTION

Due to its high efficiency and the structural advantage from the harsh environment of the ocean, ducted propellers are widely used in the offshore industries. The panel method has been proved to be an efficient and accurate tool to predict the performance of the ducted propeller with a sharp trailing edge duct. By using a viscous/inviscid interaction method, the boundary layer correction can be added to consider the viscous effect (Sun 2008, Yu 2012, Purohit 2013, Fan 2015). However, hydrofoils or propeller ducts might have a blunt trailing edge for structural reasons or to apply the anti-singing edges at high propeller radius, as shown in Figure 1. In this case, the viscous/inviscid interaction method might not work because it fails to capture the separation after the blunt trailing edge.

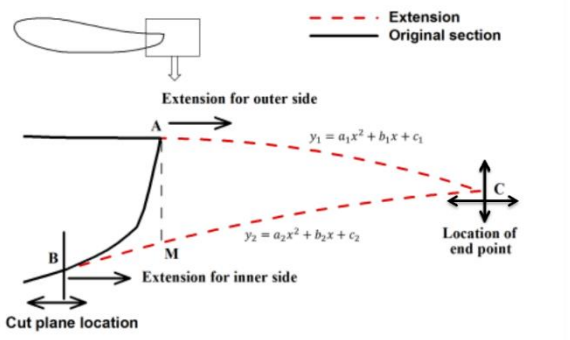

Figure 1 Duct with a blunt trailing edge and the extension scheme by Kinnas et al. (2016) (Point A and B: where the extension starts on the outer and inner side of the duct; Point C: end of the extended geometry).

The Reynolds Averaged Navier-Stokes (RANS) method can be used to handle the hydrofoils and propellers with blunt trailing edge, but this method requires much more computational resources and longer simulation time because fine grids need to be built in the downstream of the blunt trailing edge. For propellers with a blunt trailing edge duct, the whole RANS simulation can be even more challenging. Another method is to solve the duct and propeller separately in an iterative way: propeller is solved by using the vortex lattice method or the panel method, while the duct is handled by the RANS method (Kinnas et al. 2013, 2016). In the RANS method, duct can be solved in an axisymmetric solver to simplify the problem greatly. Results from this method will be used to verify the results shown in this paper.

However, for design purposes, it is meaningful to find a way to apply the panel method to hydrofoils and ducted propellers with a blunt trailing edge. One way is to modify the blunt trailing edge of the duct to a sharp trailing edge, as shown in Figure 2 (Baltazar et al. 2012). Such method is valid only if the thickness is small. If the thickness at the trailing edge is too big, this approach might change the

original geometry too much and thus fail to predict the correct flow around the duct.

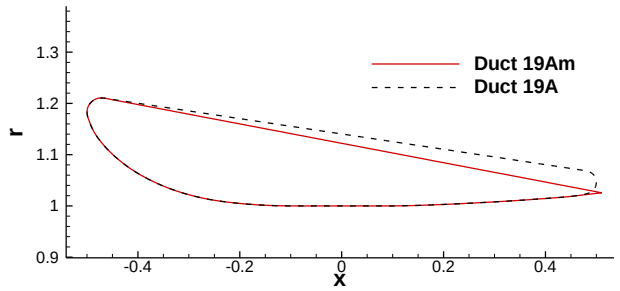

Figure 2 Original (Duct 19A) and modified (Duct 19Am) duct geometry with a round and a sharp trailing edge respectively.

Another way is to apply the extension scheme to the blunt trailing edge to extend it into the sharp trailing edge, and then implement the panel method. Previous attempts have been made by Pan & Kinnas (2011) at Ocean Engineering Group (OEG) in The University of Texas at Austin (UT-Austin). They made a vertical cut to an NACA foil to obtain a non-zero trailing edge, as shown in Figure 3. The last point of the extended geometry is moved in the vertical direction, and two kinds of criteria were used in an iterative scheme. First, the non-lift extension requires that the extended part should not provide any lift. Second, the extension was treated as a cavity surface, but with a non-constant cavity pressure distribution. This scheme was then applied in a propeller case with non-zero trailing edge thickness, and the results were compared with the experiment data.

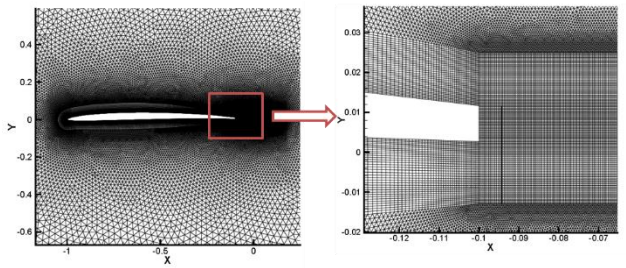

Figure 3 The hydrofoil geometry used in Pan's extension scheme (Pan & Kinnas 2011).

Purohit (2013) used the polynomial curve to represent the extended geometry and moved the last point in the vertical direction. This scheme was applied to the duct with a blunt trailing edge shown in Figure 1. However, in this scheme, the selection of Point B (where the extension starts on the inner side of the duct) and the horizontal location of Point C (last point of the extended geometry) was relatively arbitrary.

Kinnas et al. (2016) proposed another extension scheme, which contained two loops: the inner loop moves Point C in both the vertical and horizontal directions, and the non-lift and non-moment criteria were used in the Newton-Raphson method to find the coordinates of Point C; the outer loop moves point B so that it overlaps with the separation point. This scheme avoids the arbitrary selections in the previous schemes and it was applied to the geometry shown in Figure 1 as a hydrofoil case. The pressure and skin friction on the foil surface for different angles of attack were compared with the results from RANS simulations, and good correlations were observed.

In the geometry shown in Figure 1, there is one corner (Point A) with almost zero slope, and it is reasonable to start to extend the geometry from that corner on the outer side. A more general case is the geometry shown in Figure 2 with a round trailing edge. This geometry will be used as a bare duct case (the duct and propeller interaction is not considered) in this paper, and viscous pressure on the duct will be used in the improved extension scheme. The interaction between the duct and propeller is handled in the improved full wake alignment scheme in the second part of this paper, which is applied to a propeller with sharp trailing edge duct.

An improved duct wake alignment scheme is needed to properly predict the performance of the ducted propellers. Within the previous panel method, the improved wake alignment scheme called FWA has produced better performances of the ducted propeller than the cases without FWA. However, the FWA, in that case, has only been applied on the blade wake. In other words, the effects of the duct wake on the blade wake were based on the uniform distribution of the duct wake. With the cylindrical distribution of the wake panels, physical behavior of the trailing vortex of the duct wake could not be well represented.

FWA is basically based on the iterative method as described in the next section, which means the wake panels are updated at each iteration until it converges. During the iterations, very close distance between the tip of the blade wake and the duct inner side can cause the unstable convergence of the propeller performances, especially for square-tip blade. This is mainly because of the panel mismatching between the updated blade wake and the duct/duct wake. To resolve this numerical issue, repaneling process on the duct/duct wake panels is introduced, which improves not only the accuracy but also the convergence of the ducted propeller performance (Kinnas et al. 2016).

Wake alignment scheme takes a crucial role in correctly determining the spatial distribution of the free vortex sheets (simply, wake) in the downstream. The influence coefficients from the free vortex sheets to the control points on the propeller geometry are calculated based on their relative locations. Due to this reason, if wake panels are entangled during the alignment, final results will be affected due to singular behaviors among the wake panels in the panel method. A typical example of such problem is the distortion of the wake panels by the penetration of the blade wake on the duct wake. To resolve this, in this paper, the FWA is also applied on the duct wake so that the spatial distribution of the duct wake is the same as the blade wake, which is based on the local flow.

To this end, the same idea as the FWA on the blade wake is also applied to the duct wake within the framework of a low-order panel method code. Since the detailed

formulation of the wake alignment scheme can be found in (Tian & Kinnas 2012), this paper will focus on its numerical application on the steady performance of the duct wake. Before aligning the duct wake, the effects of the blade, duct, and blade wake on the duct wake are considered in terms of the induced velocity. The interactions between the blade wake and duct wake will cause the duct wake to curl near the tip of the blade wake. Results from full-blown RANS simulations will be presented for the correlations of this curling effect. Finally, the force performances from the panel method with/without the viscous effect will be compared with the experimental data for different advance ratios ranging from Js=0.30 to Js=0.50.

2 METHODOLOGY

2.1 The viscous/inviscid interaction (VII) method

The total flow field $\vec{q}$ is decomposed into an incoming flow $\overrightarrow{q_{in}}$ and a propeller-induced flow $\overrightarrow{U_{ind}}$:

$$\vec{q} = \overrightarrow{q_{in}} + \overrightarrow{U_{ind}} \tag{1}$$

In the panel method, $\overrightarrow{U_{ind}}$ can be treated as the potential flow which is governed by the Laplace's equation:

$$\overrightarrow{U_{ind}} = \nabla\phi \tag{2}$$

$$\nabla^2\phi = 0 \tag{3}$$

where ϕ is the perturbation potential.

For a hydrofoil or propeller with a sharp trailing edge, a Kutta condition needs to be satisfied:

$$\nabla\phi < \infty \text{ at trailing edge} \tag{4}$$

By using the Green's third identity, the governing equation for the panel method is given as:

$$2\pi\phi_P = \iint_{S_q}\left[\phi_q \frac{\partial G}{\partial n_q} - G\frac{\partial \phi_q}{\partial n_q}\right]ds + \iint_{S_w}\nabla\phi_w \frac{\partial G}{\partial n_w}ds \tag{5}$$

where G is the Green's function, S_q is the propeller surface and S_w is the trailing wake surface.

The classical panel method is based on the potential theory and $\overrightarrow{U_{ind}}$ is the inviscid velocity. The viscous effect can be considered by adding blowing sources on the propeller surface and the wake:

$$\overrightarrow{U_{i,vis}} = \overrightarrow{U_{i,ind}} + \sum_{j=1}^{N+N_W} C_{ij}\sigma_j \tag{6}$$

where $\overrightarrow{U_{i,vis}}$ is the viscous velocity, C_{ij} is the source influence coefficient matrix and σ is the blowing source strength, obtained by a boundary layer solver XFOIL (Drela 1989).

For a bare duct without the influence from the propeller, axisymmetric sources are used in evaluating the influence coefficients.

2.2 The improved extension scheme

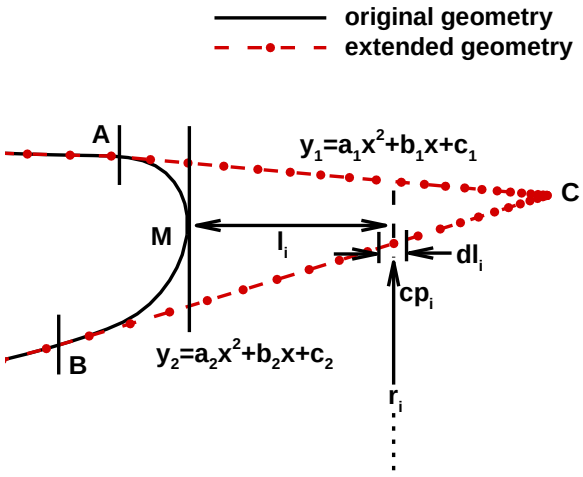

Figure 4 The improved extension scheme applied to duct with a round trailing edge using full cosine spacing (Point A, B: location to start the extension; Point C: last point of the extended geometry; Point M: original trailing edge).

The original and extended geometry are shown in Figure 4, where polynomial curves are used to represent the extended geometry. The parameters a_1, b_1, c_1, a_2, b_2 and c_2 are obtained by solving Equation set (7) to ensure both the continuity of geometry and the slope at Point A and B. For given $x_A, y_A, x_B, y_B, x_C, y_C$ and the slope at Point A and B, the solution of Equation set (7) is unique, which means the extended geometry is specified for a given original geometry and Point A, B and C.

$$\begin{cases} y_C &= a_1x_C^2 + b_1x_C + c_1 \\ y_A &= a_1x_A^2 + b_1x_A + c_1 \\ \text{slope}_A &= 2a_1x_A + b_1 \\ y_C &= a_2x_C^2 + b_2x_C + c_2 \\ y_B &= a_2x_B^2 + b_2x_B + c_2 \\ \text{slope}_B &= 2a_2x_B + b_2 \end{cases} \tag{7}$$

There are two loops in the improved extension scheme, as shown in Figure 5. The outer loop moves Point A and B until they overlap with the separation points. The inner loop uses a two-dimension Newton-Raphson method to solve for the two unknowns x_C and y_C, so two equations are needed. Once the locations of Point A, B, and C are determined, i.e. x_A, y_A, x_B, y_B, x_C, and y_C are known, the extended geometry becomes unique, and the viscous/inviscid interaction method is used to obtain the viscous pressure on the duct.

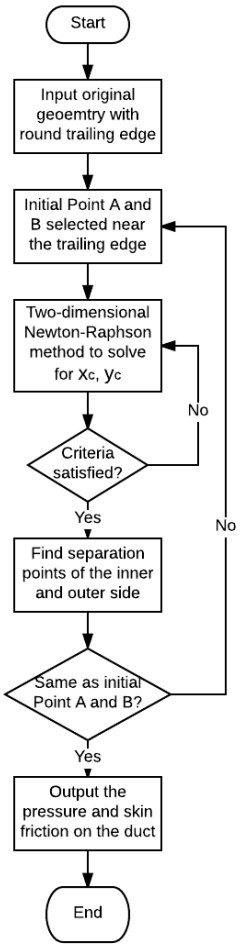

Figure 5 Flow chart of the improved extension scheme applied to duct with a round trailing edge.

Compared with the extension scheme of Pan & Kinnas (2011) and Purohit (2013), this scheme allows Point C to move in both the vertical and horizontal directions. Thus, two criteria are needed for the Newton-Raphson method to solve for the two unknowns. It is assumed that there is a separation region in the downstream of the original round trailing edge (as shown later in Figure 8 (b)), and in this region the pressure is constant. The integral of forces on both sides should be zero, yielding a non-lift criterion, as shown in Equation (8). The other criterion is the moment around Point M (the original trailing edge) of the inner and outer side is zero, which is also derived from the constant pressure assumption, as shown in Equation (9).

$$\int_{s_e} p(x)\, da = 0 \tag{8}$$

where s_e is the surface of the extended geometry (inner and outer side of the duct), $p(x)$ is the pressure at location x, and da is the infinitesimal area.

$$\int_{s_e} p(x) l(x)\, da = 0 \tag{9}$$

where $l(x)$ is the horizontal distance from location x to Point M.

As shown in Figure 4, the discretized form of the Equation (8) and (9) are:

$$\sum_{\text{inner,outer}} \sum_{\text{i}} \text{cp}_\text{i} \times dl_i \times l_i \times 2\pi \times r_i = 0 \tag{10}$$

$$\sum_{\text{inner,outer}} \sum_{\text{i}} \text{cp}_\text{i} \times dl_i \times l_i \times 2\pi \times r_i = 0 \tag{11}$$

where cp_i is the pressure coefficient, dl_i is the length in x-direction and r_i is the radius. Subscript i means theses values are at the control point on the i^{th} panel.

It should be noted that shorter extended geometry (smaller x_C) will intrinsically make the force and moment difference smaller, thus the Newton-Raphson method tends to give smaller x_C solutions. In the extension scheme proposed by this paper, the actual equations used are normalized by setting the pressure coefficient as 1 in Equation (10) and (11), as shown in Equation (12) and (13).

$$\frac{\sum_{\text{inner,outer}} \sum_{\text{i}} \text{cp}_\text{i} \times dl_i \times 2\pi \times r_i}{\sum_{\text{inner,outer}} \sum_{\text{i}} dl_i \times 2\pi \times r_i} = 0 \tag{12}$$

$$\frac{\sum_{\text{inner,outer}} \sum_{\text{i}} \text{cp}_\text{i} \times dl_i \times l_i \times 2\pi \times r_i}{\sum_{\text{inner,outer}} \sum_{\text{i}} dl_i \times l_i \times 2\pi \times r_i} = 0 \tag{13}$$

It should also be noted that in the outer loop shown in Figure 5, it is possible that there are no separation points on one or both sides of the duct, so it is hard to select the locations of Point A and B in the next iteration. In this case, a location with a relatively low skin friction is selected, and whether the final results are sensitive to the location of Point A and B is tested.

2.3 Duct wake alignment scheme using FWA

Since aligning duct wake is mainly affected by the blade wake due to the close distance between each other, duct wake alignment is conducted after the blade wake is generated at each iteration within FWA. Figure 6 describes the general flow chart of the FWA scheme including the alignment on the duct wake. Repaneling process on the duct/duct wake is also assumed to improve the final results.

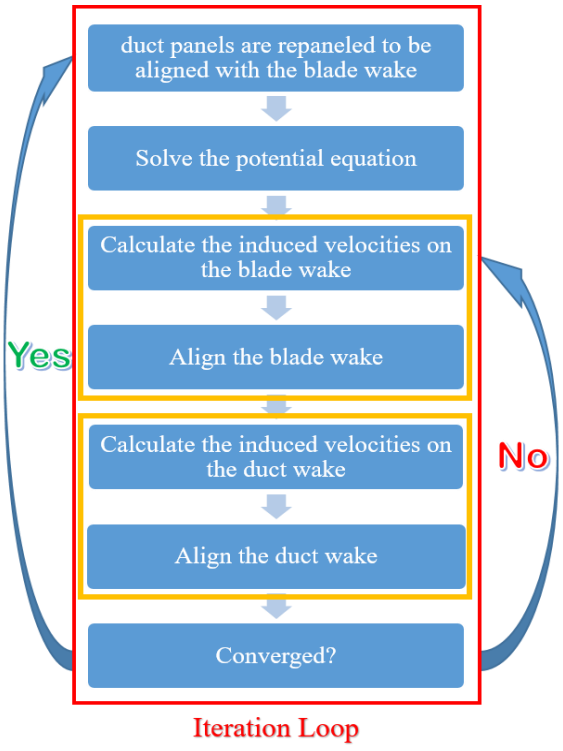

Figure 6 General flow chart of full wake alignment.

For each iteration, both the blade wake and the duct wake are aligned based on the wake geometries from the previous iteration. Both wakes can also be aligned based on the wake geometries at the current iteration step, which means both the blade wake and the duct wake are affecting each other and being aligned at the same time. Although the latter can be regarded as a complete method as it aligns the both wakes simultaneously, it produces the unstable convergence history of the final results. This instability is because of the intermediate wake geometry, which needs to go through several iterations before it gets closer to the converged shape. In other words, to avoid the abnormal induced velocities on the wake panels by using the unconverged wakes, every alignment is conducted based on the wake geometries of the previous iteration.

2.4 Induced velocity on the duct wake panels

As mentioned in the previous section, duct wake is aligned based on the effects from the duct, blade and blade wake. These effects are considered in terms of the induced velocity (or perturbation velocity) on the wake panels. The effects of duct wake on itself are also considered. In addition to the induced velocity, inflow with a rotational component constitutes the total velocity, and based on this total velocity, the four corners of the wake panels are aligned. The underlying philosophy is the same as the alignment scheme applied to the blade wake.

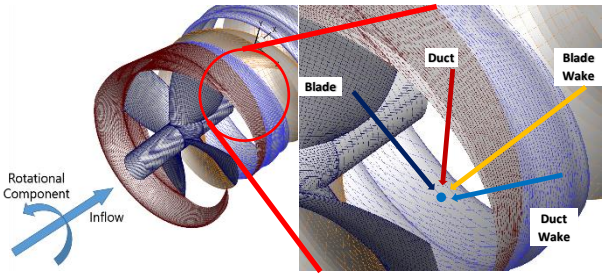

Figure 7 Ducted propeller and the induced velocity on the duct wake panels from the propeller geometry.

To improve convergence and the final results of the predicted performance, repaneling process on the duct and duct wake panels is introduced. Repaneling process will be conducted at the beginning of each iteration based on the wake geometries from the previous iteration. By using these wake geometries and the repaneled duct and duct wake, potential equations will be solved for. As a result, the convergence history of the propeller forces is improved by matching the panels on the duct inner side based on the outer edge of the blade wake. Whether matching the panels or not also highly affects the predicted loading distributions over the blade, especially toward the blade tip (Kinnas et al. 2016). By matching the panels, any singular behaviors coming from the panel mismatching between the adjacent panels can be effectively avoided.

3 RESULTS AND DISCUSSION

3.1 The viscous/inviscid interaction (VII) method

The extension scheme will be applied to a bare duct with a round trailing edge, which is shown in Figure 2 (Duct 19A). The flow field around this duct is shown in Figure 8 (a), which is from a steady axisymmetric RANS simulation with configurations shown in Table 1.

Table 1 Configurations of the RANS solver

Cell number	54.5k
Re	1×10^6
y+	<5
turbulence model	k-epsilon with enhanced wall treatment

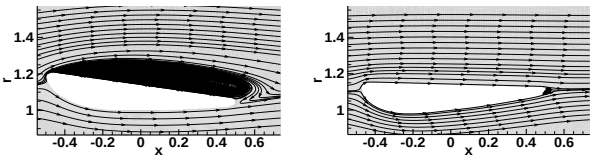

(a) Duct 19A without rotation **(b) Duct 19A rotated**

Figure 8 Flow field around the duct, predicted by the RANS method.

As shown in Figure 8 (a), there is a strong separation region on the outer side of the bare duct. To check if there is any vortex induced, an unsteady run is done with the time step being 10^{-4}s and the total simulation time being 7s. The difference between the averaged drag coefficient of the unsteady run and the drag coefficient of the steady run is within 0.1%., which proves that the flow field shown in Figure 8 is stable. As shown in Figure 9, the pressure on the inner and outer side of the original Duct 19A is close to each other, which is not favorable for the extension scheme because the force and moment differences on both sides are needed, which are based on the pressure differences.

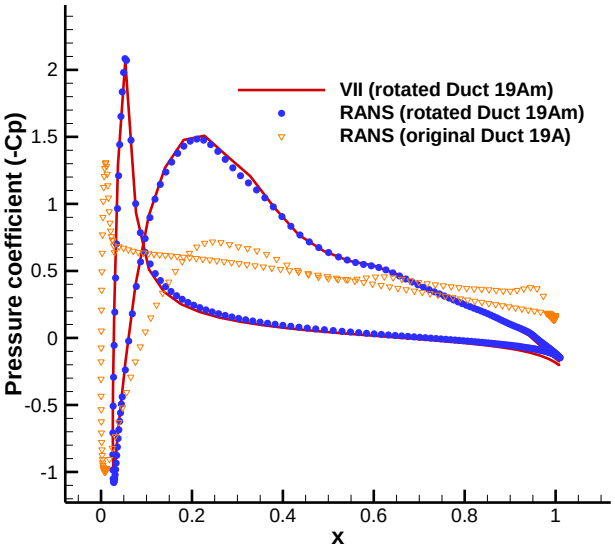

Figure 9 Pressure distributions on the duct.

To make it more appropriate and "interesting" case to test the extension scheme, the duct is rotated by 7 degrees in the counter-clockwise direction around point (0,1), where the propeller blade tip is supposed to be in the axisymmetric plane, as shown in Figure 10. The flow field around the rotated Duct 19A is shown in Figure 8 (b), and local separation can be observed after the round trailing edge, which will be represented by the extended geometry.

The extension scheme is based on the viscous pressure on the duct, which is obtained by using the viscous/inviscid interaction (VII) method. It is thus important to validate the pressure distribution from VII with the results from the RANS method for the same geometry (with sharp trailing edge and without extension, so both methods can handle it). To achieve this, Duct 19Am in Figure 2 is rotated by 7 degrees in the counter-clockwise direction around point (0,1), as shown in Figure 10. The pressure distributions on the rotated Duct 19Am from VII and RANS are shown in Figure 9, and a good correlation is found. It can be concluded that the VII method can be used solidly in the extension scheme.

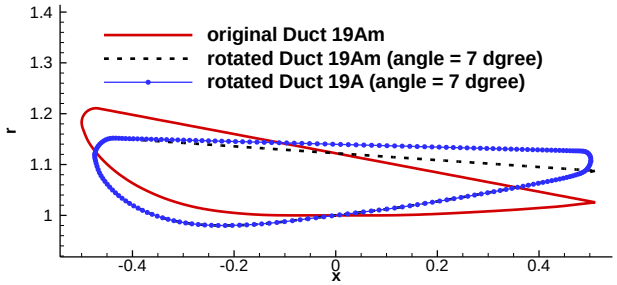

Figure 10 The ducts before and after rotation.

3.2 The improved extension scheme

The viscous/inviscid interaction method and the extension scheme are applied to the rotated duct with round trailing edge shown in Figure 10, and the pressure distribution is shown in Figure 11, compared with the results from the axisymmetric RANS method. There are some differences in the pressure distribution on the inner side of the duct for Re=10^6. The pressure correlation for Re= 10^7 is good.

In the RANS method, 8 CPUs are used and the total computational time for the case Re=10^6 is about 100s. In the VII method with the extension scheme, the computational time depends on the selection of the initial locations in the extended. However, even by using only 1 CPU, the computational time is negligible compared with the RANS method, which shows that this scheme is efficient and can be applied in the design stage of ducted propellers.

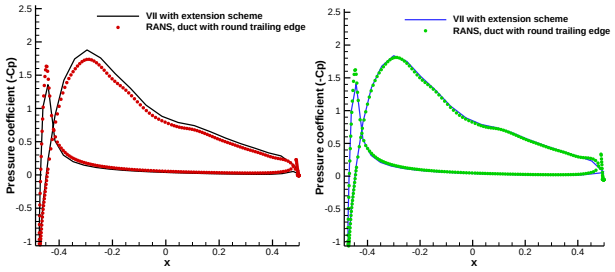

(a) Re=10^6 **(b) Re=10^7**

Figure 11 Pressure distribution from the extension scheme and the RANS method.

The skin frictions predicted from both methods agree well, as shown in Figure 12. In the viscous/inviscid interaction method, the skin friction near the leading edge is not as smooth as those from the RANS method.

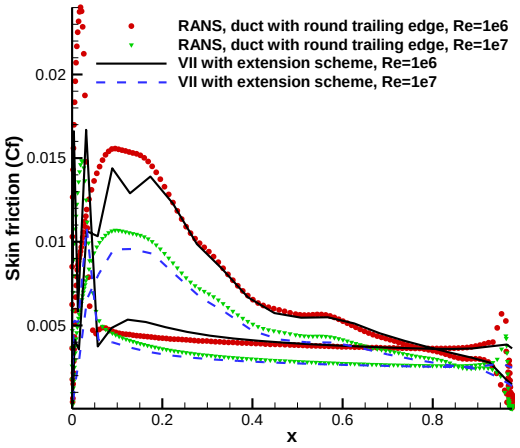

Figure 12 Skin friction on the duct from the extension scheme and the RANS method.

The extension scheme converges within a few iterations, and the convergence history for the extended geometry is shown in Figure 13. The corresponding pressure distributions are shown in Figure 14, and the extended geometry will influence the pressure distribution on the whole duct, i.e., the influence on the pressure is not local, so a proper extension scheme is important. It is also shown that the pressure distribution on the duct is more sensitive to the movement of Point C in the vertical direction than the horizontal direction.

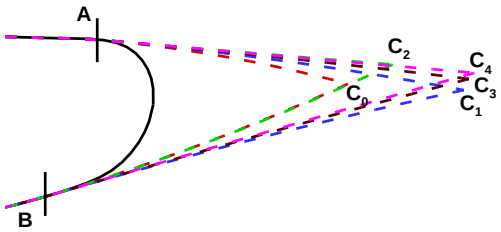

Figure 13 The convergence history of the extended geometry (Re = 10^6).

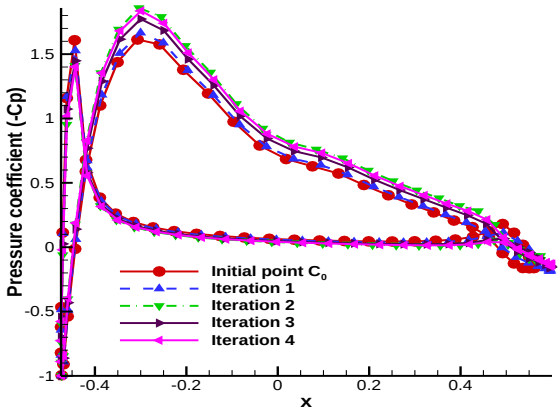

Figure 14 The convergence history of the pressure distribution.

It should be noted that the skin friction does not go to zero in this case, which means there is no separation in the extended duct. Figure 13 shows that both the inner and outer side of this duct near the trailing edge are relatively flat, so the results of the extension scheme are not sensitive to where the extended geometry starts, as long as Point A and Point B do not fall into the "round" part of this

geometry. However, for the duct shown in Figure 1, the outer loop of the scheme is important in determining the position of Point B on the inner side of the duct.

3.3 Ducted propeller with a square tip blade and a sharp trailing edge duct

To validate the predicted performance of the ducted propeller from panel method, ducted propeller with a square tip blade (KA4-70) and a sharp trailing edge duct (19Am, as shown in Figure 2) is adopted. Figure 15 shows the geometry of the ducted propeller.

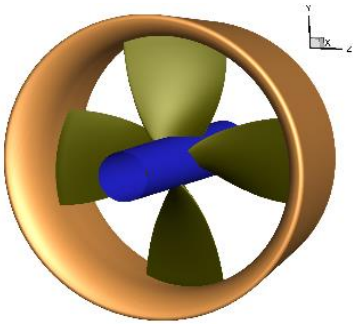

Figure 15 Geometry of the ducted propeller with a square tip blade.

Force performances are correlated with the experimental data (Bosschers 2009). In this paper, more emphasis will be on the distribution of the wake panels behind the duct and the blade trailing edge. This will be intensively investigated with the correlations between the results from the panel method and the RANS simulations. Predicting the correct location of the shedding vortex (or wake) in the downstream is a prerequisite of predicting the correct propeller performance, because the distribution of the wake panels highly affects the final results. For example, the aligned blade wake near both the duct inner side and the duct wake can penetrate those geometries. In that case, the penetration can cause singular behaviors on both the blade and the duct wake panels, resulting in the distortion of the wake panels. The effects of the blade wake on the predicted propeller forces were also addressed in Hongyang (2015). In that paper, the force performances using the simplified shape of the blade wake deviated from both the experimental data and the results from the panel method with FWA. However, the latter two results were in good agreements each other.

3.4 Two-dimensional contour plot of shedding vortex from RANS simulations

For the validation of the distributed wake from the panel method with FWA, the two-dimensional contour plots of vortex magnitude from RANS simulations are adopted. The correlations will be performed for a range of the advance ratio from 0.3 to 0.5. Figure 16 and Table 2 show mesh gridding of the ducted propeller and the parameter settings in the RANS simulations respectively. In Figure 16, only a quarter of the whole geometry is presented since periodic boundary condition is used in the RANS simulations. Also, a cut in the x-y plane in Figure 16 will be used to plot the two-dimensional contour of the shedding vortex from the RANS simulations.

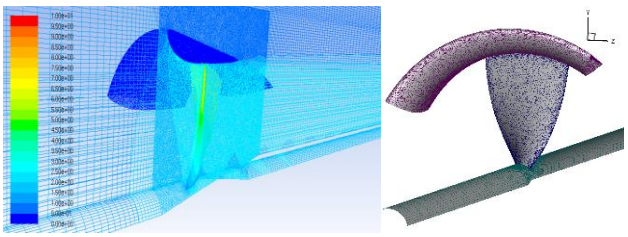

Figure 16 The gridding of blade and duct in the RANS simulation (right) and the two-dimensional plane cutting through the geometry with a constant angle of zero degrees (left).

Table 2 Parameter setting in RANS simulations and computational time, adjusted from Table 4.1 of Fan (2015)

Cell Number	Over 6 million
Reynolds Number	1.0E+6
Turbulence Model	$\kappa - \varpi$ SST
Pressure Correction Scheme	*SIMPLEC*
Spatial Discretization	*QUICK*
CPU Type	Intel Xeon 2.54 GHz CPU
Calculation Time (32 CPUs)	Over 32 Hours

Two-dimensional contour plots are presented in Figure 17 for a range of advance ratios from 0.3 to 0.5. As seen from the figures below, the higher the advance ratio is, the more shedding vortex behind the propeller geometries diffuses. Also, the case with the lower advance ratio shows stronger shedding vortex near the trailing edge of duct than the case with the higher advance ratio. The shedding vortex gradually diffuse as it flows into the downstream with local flow.

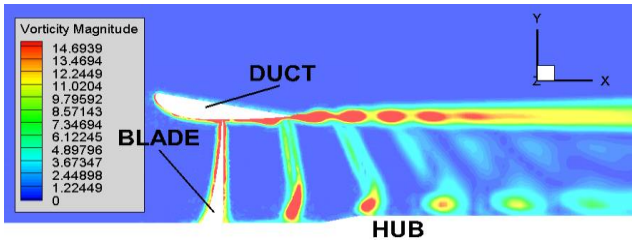

(a)

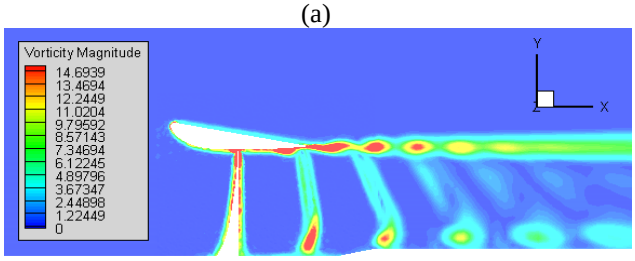

(b)

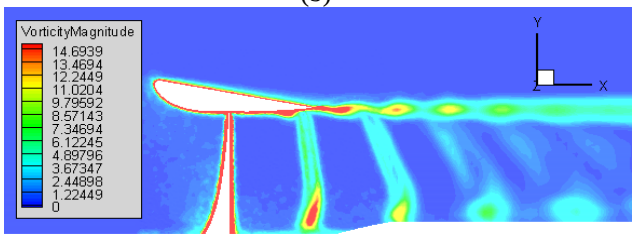

(c)

Figure 17 Two-dimensional contour plots of the propeller geometry and shedding vortex with diffusion for advance ratios of 0.3 (a), 0.4 (b), and 0.5 (c).

3.5 Two-dimensional contour plot of concentrated shedding vortex from the panel method

In panel method, vortex shed from both the duct and the blade trailing edge is represented by the distribution of the wake panels. Since diffusion effects of the shedding vortex cannot be represented by the planar panels in the panel method, the diffused shedding vortex will be replaced by the concentrated vortex. Then, the concentrated vortex will be placed on the wake panels, which are to be distributed based on the local flow velocity from FWA. Now that the FWA is based on the iterative method, it will take several iterations for the aligned wake to reach the fully converged shape. Figure 18 presents the convergence history of the wake panels during the wake alignment scheme applied on both the duct and the blade wake, with a design advance ratio of 0.5. Two-dimensional plots based on the planes cutting through the center of the propeller geometry are also presented to show the detailed distribution of the wake panels during the iterations.

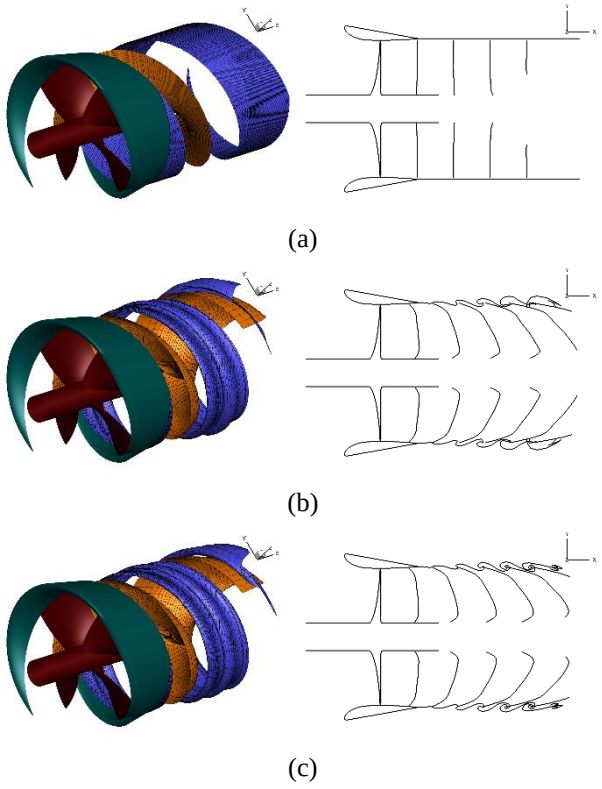

(a)

(b)

(c)

Figure 18 Convergence history of the full wake alignment scheme applied to both the blade and the duct wake (only part of the propeller geometry is shown for clarity) at the (a) 1st, (b) 5th, and (c) last iteration out of 30 loops.

As can be seen from the figures above, FWA starts its first iteration based on the helical and cylindrical shapes for the blade wake and duct wake respectively. Then, the solutions based on these initial geometries will be used as a basis for the next iteration until the FWA reaches its convergence criteria.

Now, Figure 19 shows the correlation of the wake distributions between the results from the panel method and RANS simulations. The range of the investigated advance ratios is from 0.3 to 0.5. The locations of the concentrated vortex from the panel method are in very good agreements with those of the shedding vortex predicted by RANS simulations. These agreements are more addressed especially near the duct trailing edge. Also, the curling behavior of duct wake due to its close distance to the tip of the blade wake is well predicted by both methods, and a good correlation is observed. This curling comes from the strong tip vortex, which is shed from the blade tip and therefore located at the tip of the blade wake. As in the figures below, the strength of the curling gets weaker as the shedding vortex flows into the downstream due to diffusion. The same happens to the shedding vortex from the blade as it flows along with the local flow.

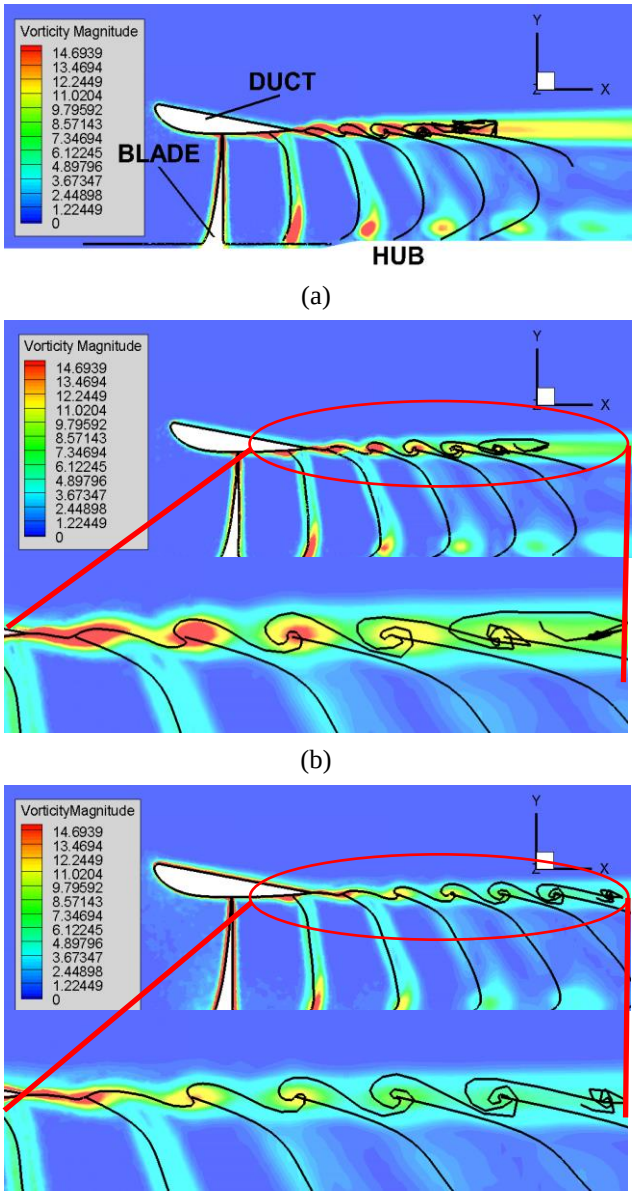

(a)

(b)

(c)

Figure 19 Correlations of the two-dimensional contour plots of the shedding vortex and propeller geometry between the results from RANS simulation and panel method (black solid line) for advance ratios of 0.3 (a), 0.4 (b), and 0.5 (c).

The curling behavior of the wake panels is well represented near the duct trailing edge where the shedding vortex starts to separate. However, in the region where the shedding

vortex gets spread such as the downstream, distribution of the wake panels from FWA cannot represent well the diffusion effects especially at the lower advance ratios. Due to this drawback, panel method only considers and represents the shedding vortex up to the region where it is not widely spread. Considering the far distance between the propeller geometry and the ignored shedding vortex, the effects of the ignored vortex on the final results are negligible.

3.6 Predicted force performance from panel method and experiment

The overall force performances, i.e. thrust and torque on the blade and duct are compared with the experimental data for the advance ratios from 0.3 to 0.7, as shown in Figure 20. Results from the panel method are inviscid, which mainly reduces the predicted torque. The viscous effect can be considered by using empirical corrections to the pitch angle of the blade, which applies a constant friction coefficient to include an approximate friction force (Kerwin & Lee 1978). Another way is to use the viscous/inviscid interaction method and solve the boundary layer equations along each blade section. Both viscous effect corrections can predict the torque much closer to the results of the experimental measurement, as shown in Figure 20. However, the viscous/inviscid interaction method can improve the pressure prediction on the propeller blade (Sun 2008, Yu 2012).

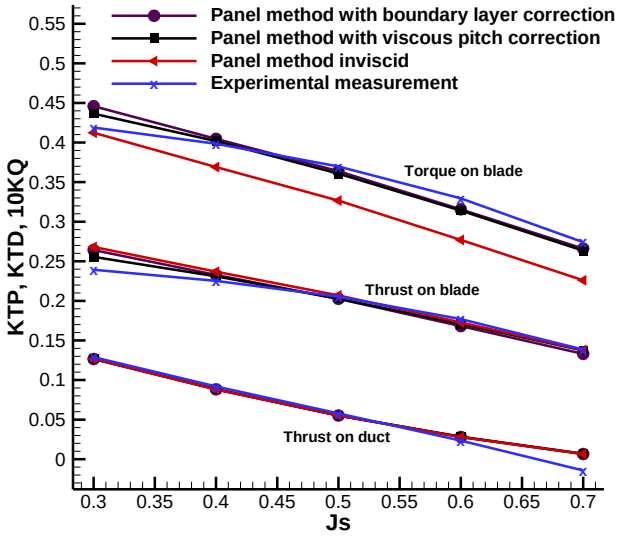

Figure 20 Correlation of the predicted force performance of the KA4-70 ducted propeller between the experiment and the panel method using full wake alignment with/without viscous corrections.

The figure shows that the predicted forces from the panel method with viscous corrections and by using FWA on the both blade and duct wake are in good agreements with the experimental values over the most advance ratios. Compared to the results previously presented by Ocean Engineering Group (Kinnas et al. 2016), the overall force performances presented here somewhat deviate from the experimental values. This might be due to the fact that the previous results were based on the cylindrical shape of the duct wake, while the current method includes the wake alignment on the duct wake as in the case of the blade wake. The relative locations between the blade wake and duct wake after the alignment might affect the final results, which needs further investigation in the near future.

3.7 Pressure distribution on duct

The pressure distribution over duct geometry calculated by the panel method is correlated with the results from both RANS simulation and RANS/VLM coupling method (Kinnas et al. 2013) at the design advance ratio, *Js*=0.50. The RANS/VLM coupling method, developed by OEG at UT-Austin, couples a potential flow based vortex-lattice method (VLM) with an axisymmetric-swirl RANS solver for the analysis of the performance of propulsors. More details of this coupling method are left aside in this paper and are described in (Kinnas et al. 2013).

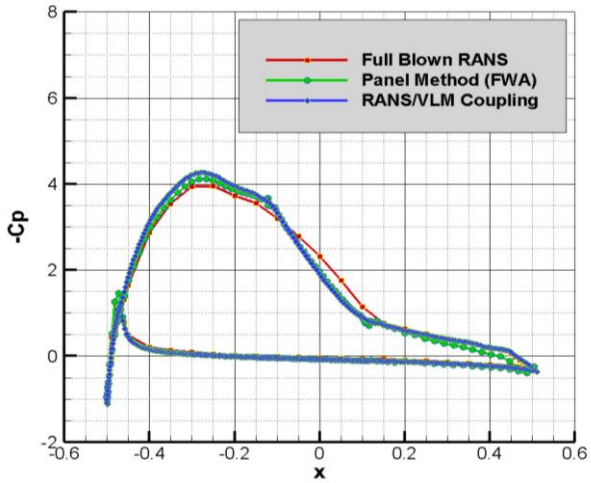

Figure 21 Correlation of the predicted pressure distribution on the duct between the panel method, coupling method, and RANS simulation.

As shown in Figure 21, the prediction of the pressure distribution by the panel method is in very good agreement with the RANS/VLM coupling method. Only the result from RANS simulation slightly deviates from the other two methods, even though not considerably.

4 CONCLUSION AND FUTURE WORK

In this paper, the viscous/inviscid interaction method is firstly applied on bare duct with sharp trailing edge, and a good correlation with the RANS method is observed. Based on this, an improved extension scheme is proposed, in which the separation region is represented by the extended geometry. A two-dimensional Newton-Raphson method is used for the inner loop of this scheme, and none-force & none-moment criteria are adopted to allow the last point of the extension to move in both the vertical and horizontal direction. This method is applied to duct with round trailing edge and the pressure distribution and skin friction are well correlated with the results from the RANS method. It is shown that the extended geometry has an influence on the overall pressure distribution, thus a proper extension scheme is important. This method is also shown to be much more efficient compared with the RANS method, which allows it to be applied to the design stage of the ducted propeller in the future.

To address the influence between the propeller blade and the duct, the full wake alignment (FWA) method has been applied on the ducted propeller with a square tip blade and a sharp trailing edge duct. This paper concisely introduced the iterative algorithm built in the FWA. By using the alignment scheme, not only the blade wake but also the duct wake is aligned based on the local flow in the downstream. By aligning the duct wake, current panel method can represent the behavior of the shedding vortex behind the propeller geometry. To validate this, the location of the shedding vortex has been correlated with the results from RANS simulations. As a result, not only the locations but also the curling behaviors of the wake are in very good agreements between each other except the region where the wakes highly diffuse in the downstream. By using the viscous pitch correction and the viscous/inviscid interaction method in the panel method, the viscous effect is included, which significantly improves the correlation with the experiment data in the torque prediction. The predicted force performances are somewhat deviated from the experimental data at the high loading, remaining further investigation on the effects of the aligned wakes on the force performances.

In the future, the alignment model will be applied to other ducted propeller geometries, including those with round tip blade, as well in the case of cavitating flow.

REFERENCES

Bosschers, Ir. J. (2009). 'Open Water Tests for Propeller KA4-70 and Duct 19A with a Sharp Trailing Edge'. Technical Report, MARIN, Report No. 22457-2-VT.

Baltazar, J., J. A. C. Falcão de Campos & J. Bosschers (2012). 'Open-water thrust and torque predictions of a ducted propeller system with a panel method'. International Journal of Rotating Machinery. Vol. 2012. Article ID 474785.

Drela, Mark (1989). 'XFOIL: An analysis and design system for low Reynolds number airfoils'. In Low Reynolds number aerodynamics, pp. 1-12. Springer Berlin Heidelberg.

Fan, Hongyang (2015). 'An Improved Panel Method for the Prediction of Performance of Ducted Propellers'. MS thesis, Ocean Engineering Group, the University of Texas at Austin.

Kerwin, Justin E., and Chang-Sup Lee (1978). 'Prediction of steady and unsteady marine propeller performance by numerical lifting-surface theory'. Transactions of Society of Naval Architects & Marine Engineers **86**

Kinnas, Spyros A., Jeon, Chan-Hoo, Purohit, Jay & Tian, Ye (2013). 'Prediction of the unsteady cavitating performance of ducted propellers subject to an inclined inflow'. International symposium on marine propulsors SMP, Vol. 13.

Kinnas, Spyros A., Su, Yiran, Du, Weikang & Kim, Seungnam (2016). 'A viscous/inviscid interactive method applied to ducted propellers with ducts of sharp or blunt trailing edge'. 31st Symposium on Naval Hydrodynamics, Monterey, USA.

Pan, Yulin. & Kinnas, Spyros A. (2011). 'A viscous/inviscid interactive approach for the prediction of performance of hydrofoils and propellers with nonzero trailing edge thickness'. Journal of Ship Research, Vol. 55, No. 1, pp. 45-63.

Purohit, Jay Bharat (2013). 'An improved viscous-inviscid interactive method and its application to ducted propellers'. MS Thesis. Ocean Engineering Group, the University of Texas at Austin.

Sun, Hong (2008). 'Performance prediction of cavitating propulsors using a viscous/inviscid interaction method'. Ph.D. Thesis. Ocean Engineering Group, the University of Texas at Austin.

Tian, Ye & Kinnas, Spyros A. (2012). 'A wake Model for the Prediction of Propeller Performance at Low Advance Ratios'. International Journal of Rotating Machinery Volume 2012, Article ID 372364.

Yu, Xiangming (2012). 'Three dimensional viscous/inviscid interactive method and its application to propeller blades'. MS Thesis. Ocean Engineering Group, the University of Texas at Austin.